

Energy dissipation statistics in the random fuse model

Clara B. Picallo^{1,2,*} and Juan M. López^{1,†}

¹*Instituto de Física de Cantabria (IFCA), CSIC-UC, E-39005 Santander, Spain*

²*Departamento de Física Moderna, Universidad de Cantabria, Avenida Los Castros, E-39005 Santander, Spain*

(Received 23 October 2007; revised manuscript received 19 February 2008; published 21 April 2008)

We study the statistics of the dissipated energy in the two-dimensional random fuse model for fracture under different imposed strain conditions. By means of extensive numerical simulations we compare different ways to compute the dissipated energy. In the case of an infinitely slow driving rate (quasistatic model), we find that the probability distribution of the released energy shows two different scaling regions separated by a sharp energy crossover. At low energies, the probability of having an event of energy E decays as $\sim E^{-1/2}$, which is robust and independent of the energy quantifier used (or lattice type). At high energies, fluctuations dominate the energy distribution, leading to a crossover to a different scaling regime, $\sim E^{-2.75}$, whenever the released energy is computed over the whole system. On the contrary, strong finite-size effects are observed if we consider only the energy dissipated at microfractures. In a different numerical experiment, the quasistatic dynamics condition is relaxed, so that the system is driven at finite strain load rates, and we find that the energy distribution decays as $\mathcal{P}(E) \sim E^{-1}$ for all the energy range.

DOI: 10.1103/PhysRevE.77.046114

PACS number(s): 46.50.+a, 62.20.M-

I. INTRODUCTION

Acoustic emission (AE) in fracture is an example of a broader phenomenon known as “crackling noise” [1]. A system crackles in response to an external stimulus, leading to energy dissipation in the form of avalanches of events with no characteristic size. Examples can be found in volcanic rocks [2], crumpling paper [3], superconductors [4], disordered magnets [5], or plastic deformation of materials [6]. The release of acoustic energy in fracture experiments is related to irreversible processes, like creation of microcracks and deformation.

AE experiments in stressed materials typically give a power-law distribution of the dissipated energy, $\mathcal{P}(E) \sim E^{-\beta}$, as the system is slowly driven toward catastrophic failure. This can be seen as a small-scale analog of the Gutenberg-Richter law for earthquakes. The exponent β is found to depend on the material, and in the literature one can find $\beta \approx 1.3$ in synthetic plaster [7], $\beta \approx 1.25$ in paper [8], $\beta \approx 2.0$ in fiberglass and $\beta \approx 1.51$ in wood [9–11], $\beta \approx 1.5$ in cellular glass [12], and $\beta \approx 1.8$ in paper peeling experiments [13]. This spread of values indicates that the exponent is not universal and it may depend on the material characteristics as well as on the loading conditions.

In simple discrete models the scale-free response is associated with a cascade of local failures. As the external load is slowly increased, weak elements fail to hold the imposed local stress and break. Some internal load redistribution mechanism, whose details depend on the particular model, increases the local stress on the remaining elements and may cause further simultaneous local failures. As a result, the material may respond in avalanches of failure events whose size distribution is often very broad.

For obvious reasons AE is a very useful nondestructive tool that, if properly understood, may give crucial informa-

tion about the damage accumulated in loaded materials. Indeed, mean-field calculations and simulations in some simplified models indicate that the energy statistics follows a power law with an exponent that changes as the catastrophic failure point is reached [14,15]. Events recorded near global failure show a power-law decay with an exponent distinctly smaller than those events recorded far away from the breakdown point. Interestingly, recent experiments on granite under different loading conditions have shown a qualitative agreement with this theoretical observation [16]. Should this be a robust and universal property it could be potentially used as a tool to easily diagnose the damage in loaded materials.

Scaling in fracture is apparently very generic and can also be observed in other quantities (see, for instance, Ref. [17] for a recent review). The distribution of quiet times between AE events also obeys a power-law analog of the Omori law for earthquake occurrence [8,10–12,16,18,19]. Scale-invariant behavior is also observed in the height-height correlations of fracture surfaces [17]. The existence of scaling laws in experiments suggests an interpretation in terms of critical behavior as the global failure point is approached. However, results are not conclusive and a straightforward link between experiments and models is still lacking.

From a theoretical point of view, fracture physics is a challenging open problem. Materials are heterogeneous and disorder details may play a crucial role. However, the existence of power-law behavior makes it appealing to try to describe fracture with very simplified models that include the most relevant symmetries, dimensionality, disorder features, and loading conditions.

There has been a great effort devoted to describing fracture crack surfaces in a simple way by means of stochastic field equations for the dynamics of an advancing front, where the crack is modeled as an elastic string driven through a disordered medium in the presence of nonlocal interactions [20–24]. However, continuous crack line models have failed to fully agree with experiments, seemingly because certain important aspects of fracture, like nucleation of

*picallo@ifca.unican.es

†lopez@ifca.unican.es

voids in the advancing front, are not addressed in these continuum approaches. In this respect, lattice models are expected to be more appropriate. Lattice models describe the elastic solid as a network of springs with random failure thresholds where the displacement field can be either scalar or vector. In particular, the random fuse model (RFM) [25] has attracted a lot of attention as a minimal model for fracture since it is capable of reproducing some essential features of the fracture phenomenon in a very simple setting. The RFM represents a scalar electrical analog of the elasticity problem. This correspondence is based on the formal equivalence between the mathematical form of the generalized Hooke's law for the scalar elastic problem, $\sigma_i = \sum_j g_{ij} \epsilon_j$, and the equations for the electrical problem, $\gamma_i = \sum_j k_{ij} v_j$, where the stress (σ), local elastic modulus (g), and strain (ϵ) can be mapped to the current density (γ), local conductance (k), and local potential drop (v), respectively. This model goes one step further than mean-field models, like the fiber bundle model, by including local distribution of stress between the nodes, while preserving the simplicity in the introduction of disorder as a distribution of thresholds in the system. Much attention has been devoted to the RFM in the last two decades, including studies concerning the influence of disorder [26,27], presence of multiscaling behavior in voltage and current [28], roughness exponents [26,29–32], damage localization [33], and failure avalanche distributions [15,30,34–38]. Interestingly, an experimental realization of the RFM has recently been studied [39] to investigate the influence of disorder on the I - V characteristic and crack length.

The dynamics of the RFM takes place in the form of avalanches of failure events. Therefore, it is tempting to link avalanche activity to the AE observed in experiments. Several studies have focused on the statistics of avalanches of failure events in the fuse model [15,34–36] and improved simulation algorithms have recently allowed to study larger systems with much better statistics [30,37,38]. However, numerical determinations of the energy exponent β under different loading rates or on different lattices are scarce.

Lattice models typically predict larger energy exponents β than those obtained in experiments. A number of reasons might be responsible for this discrepancy, including the brittle nature of the models, the existence of dispersion of acoustic waves in experiments, or the lack of an effective time scale separation between stress relaxation and loading in real systems, which is assumed in quasistatic models.

Here we study the statistics of the dissipated energy in the RFM under different imposed strain conditions. We compare seemingly equivalent definitions of the dissipated energy. For an infinitely slow driving rate (quasistatic model) we find that the probability distribution function (PDF) of the released energy shows two different scaling regions. For low energies, the dissipated energy distribution is robust and independent of the lattice geometry. We find $\mathcal{P}(E) \sim E^{-1/2}$ and a simple scaling argument is given to explain this behavior. However, at high energies the distribution exhibits a cross-over to a regime where $\mathcal{P}(E) \sim E^{-2.75}$, whenever the energy losses are evaluated over the whole volume of the system. We also study a different estimator of the dissipated energy that takes into account the energy losses occurring only at

microfractures. This microscopic estimator exhibits strong finite-size effects and fails to show critical behavior. In a different setting, when the system is driven at finite strain load rates, we find that the energy distribution decays as $\mathcal{P}(E) \sim E^{-1}$ for all the energy range.

The paper is organized as follows: In Sec. II we define the model; in Sec. III we discuss the dissipated energy and ways to measure it and we report on our results for quasistatic and nonquasistatic dynamics in the fuse model. Finally, we conclude with a discussion in Sec. IV.

II. THE RANDOM FUSE MODEL

We study a two-dimensional lattice of fuses with unit conductivity $k_j=1$ and a disordered threshold current γ_j^{th} that is a quenched random variable from a uniform probability distribution in the interval $(0,1)$. An external voltage is imposed between two bus bars placed at the top and the bottom of the system, and periodic boundary conditions are imposed in the horizontal direction. The system can be driven by a slowly increasing voltage or current, mimicking the experimental situation where either strain or stress load can be imposed, respectively. At each update, the Kirchhoff voltage equations are solved to determine the currents flowing in the lattice. All fuses with current exceeding the corresponding local threshold are blown and, once the entire system is below threshold, the voltage (current) is again increased. An avalanche of failure consists of all the fuses blown between two external voltage (current) increments. Each fuse behaves linearly until the local current γ_j reaches the threshold. Then, the fuse burns and irreversibly becomes insulating $k_j=0$, so that burnt fuses are no longer able to carry any current. The current is redistributed instantaneously after a fuse is burnt so that current relaxation occurs in time scale that is much faster than the driving time scale. In our simulations, voltage driving is imposed. The described configuration should be compared with experimental setups in mode-I fracture where the strain is slowly increased. An experimental comparison of the AE and critical behavior of fracture precursors for different load features (strain vs stress loading) and geometries has been reported in Ref. [10]. Although imposed strain experiments indicate an induced plastic deformation in the final stages, no differences were encountered in AE distribution between the two different loading conditions.

The need to solve a large system of linear equations for each update implies a high computational cost and limited the reachable system size and the statistical sampling in this model in the past, when the best performance was achieved by conjugate gradient methods [40]. Recently, a new algorithm based on a rank-1 downdating of sparse Cholesky factorizations has been introduced [41,42], which can greatly reduce the computational cost of the simulations. Here we make use of this algorithm to study two-dimensional networks of fuses in triangular and diamond lattices. We studied systems of linear size ranging from $L=16$ to 256 and 10^4 realizations of the disorder.

III. DISSIPATED ENERGY

In stressed materials, elastic energy is stored due to redistribution of the external load all across the lattice. Energy

dissipation in the RFM occurs in bursts of breaking events which can be compared with the AE observed in experiments. In doing so, one is assuming that the main contribution to AE is given by the dissipated elastic energy, while dislocations and friction are, in a slowly driven experiment, secondary contributions to AE. Also, it is worth keeping in mind that in real systems one expects that only a fraction of this dissipated energy leads to the AE observed, while the remaining losses are due to other dissipative mechanisms like dispersion or damping of acoustic waves, which are not described by purely elastic models like the RFM. Several ways to define the dissipated energy can be envisaged, as we discuss below.

Pradhan *et al.* [15] found that $\beta=2.7$ for the RFM on diamond lattices under stress loading conditions. They calculated the electric power dissipation in the fuse model as the product of the voltage drop across the network and the total current that flows through it. The power dissipation in the electrical model is equivalent to the stored elastic energy in a mechanical system. This is a global definition that assumes that the whole volume of the system contributes to the dissipated energy.

Alternatively, following Salminen *et al.* [8], we can define the energy lost during a given avalanche event n as

$$E_n \sim V_n^2 \Delta G_n \sim V_n^2 s_n, \quad (1)$$

where ΔG_n is the change in the elastic modulus due to the failure avalanche, s_n is the number of broken bonds (avalanche size) of the n th event, and V_n is the corresponding potential drop between the bus bars (strain imposed in the sample). This definition makes use of the global strain imposed on the system and can be seen as a coarse-grained or *macroscopic* measure of the dissipated energy.

Note that the definitions of both Pradhan *et al.* [15] and Salminen *et al.* [8] of the dissipated energy take into account the whole volume of the system. However, there is strong experimental evidence indicating that AE is actually a localized phenomenon in space and time so that energy release actually occurs at microfractures [9,10], and it is not therefore spread across the system. This suggests that one should consider other ways to define the dissipated energy in the model; in particular, it may be interesting to study measures of released energy that are directly linked to the bonds involved in avalanches of local breaking events.

In this spirit, we introduce here what we call *microscopic* dissipated energy, which is defined as the sum of the energy losses at every element of the system involved in the n th failure avalanche. This can be calculated by adding up the energy dissipated by each individual broken bond, $\gamma_j = k_j v_j^2$, where v_j is the local potential drop at bond j . Since fuses break right at the threshold, we can define the *microscopic* dissipated energy due to the n th failure avalanche as

$$E_n = \sum_j^{s_n} (\gamma_j^{\text{th}})^2, \quad (2)$$

where the sum runs over each broken bond within the n th avalanche.

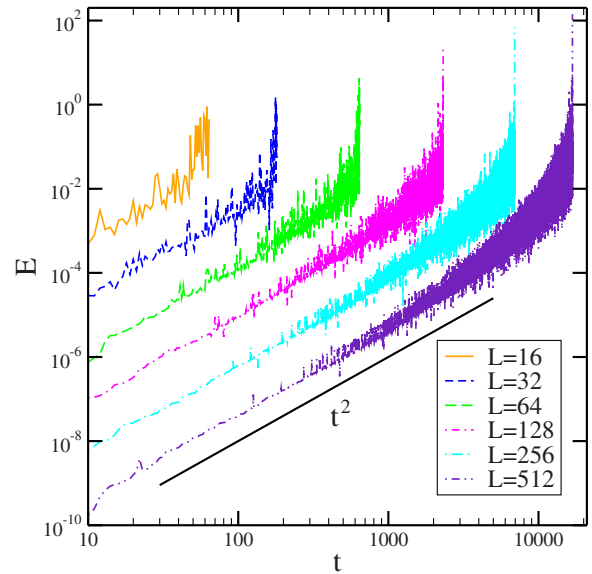


FIG. 1. (Color online) Temporal evolution of microscopic energy until breakdown for a typical realization of the disorder on diamond lattices ranging from $L=16$ (top curve) to 512 (bottom curve). A first region with slope $\alpha=2$ is followed by a second region dominated by fluctuations.

We devote the rest of the paper to analyzing the dissipated energy statistics in the fuse model for the case of infinitesimal strain (quasistatic model) and also under different finite strain rates (nonquasistatic model). We shall be comparing the numerical results for the different measures of the dissipated energy discussed above for triangular and diamond lattices. One would expect that the three definitions give similar temporal behavior for the dissipated energy statistics, apart from constant factors. Although this is actually the case in the low-energy range, dissipation statistics differs at high energies for different estimators.

A. Quasistatic case: Infinitesimal strain rate

Let us first focus on infinitesimal driving. For the sake of computational convenience, a voltage $V=1$ is fixed between the two bus bars. The next fuse to burn is determined by $\max_j(\gamma_j/\gamma_j^{\text{th}})$ so the external voltage is increased until this fuse exactly reaches its threshold. The new current configuration is calculated according to Kirchhoff equations. This rearrangement can cause other fuses to overpass their thresholds without further voltage increase. All the fuses burnt at the same external voltage constitute an avalanche. This process is repeated until the network becomes disconnected.

Quasistatic dynamics results in two very well-separated time scales, i.e. a fast relaxation process and a slow external driving. As occurs in other systems exhibiting a well-defined time scale separation (as for instance in self-organized criticality), the natural time scale is given by the slow time scale. Therefore, in the following, time refers to the number of avalanches that have occurred. In Fig. 1 we show a typical realization of the temporal evolution for the dissipated energy according to Eq. (2) for different system sizes. One can see that for each realization the released energy grows in

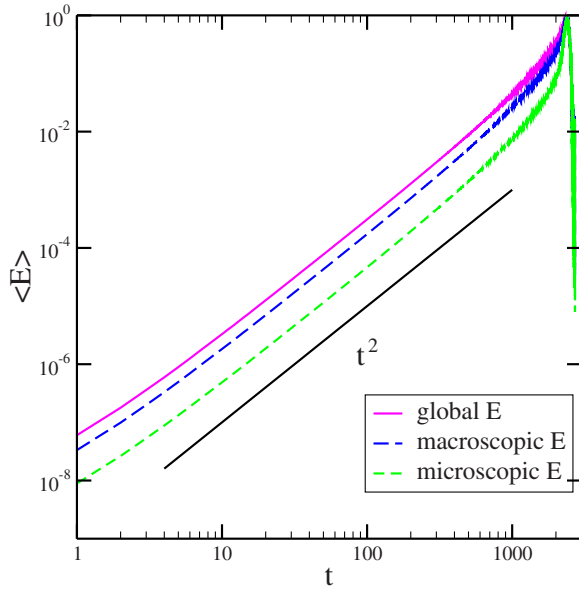


FIG. 2. (Color online) Temporal evolution of energy dissipation averaged over 10^4 realizations in an $L=128$ diamond lattice. All three energies, global, macroscopic, and microscopic, exhibit the same t^2 trend. The three curves have been rescaled by its maximum for clarity.

time as a power law, $E(t) \sim t^2$. At later times, fluctuations around the trend increase (the larger, the bigger the system size) as the system approaches the total breakdown point. This dynamic behavior is very robust and independent of the system size or lattice type.

We also found identical temporal behavior for the macroscopic dissipated energy, Eq. (1), and for the dissipated electric energy used by Pradham *et al.* for both diamond and triangular lattices. In Fig. 2 we compare the temporal evolution of the average dissipated energy on the diamond lattice according to the three definitions. Notably, this behavior is also in agreement with that reported in Ref. [43] for a very different dynamical spring model that included acoustic waves. The origin of the robust t^2 growth law is perhaps more transparent in Eq. (1), where the driving potential is increasing linearly with time (as we are imposing a quasi-static dynamics).

The temporal power-law trend gives significant information about the functional form of the dissipated energy statistics in the RFM. The probability density function of the dissipated energy at time τ in a system of lateral size L is given by $\mathcal{P}_\tau(E, L) = (1/\tau) \int_0^\tau dt \delta[E(t, L) - E]$, where $\delta(u)$ is the Dirac delta distribution. This corresponds to the energy distribution to be observed after the first τ avalanche events. Note that the probability distribution $\mathcal{P}_\tau(E, L)$ is expected to be nonstationary, so it should depend explicitly on the observation time τ . Let us now consider that the dissipated energy grows in time as a power-law with some exponent, $E(t, L) \sim L^{-\sigma} t^\alpha + \eta(t)$, where σ captures the scaling with system size observed in Fig. 1 and $\eta(t)$ is a noise term representing the random fluctuations around the trend. The details of the noise term $\eta(t)$ are not known, but one can argue that they may depend nontrivially on the interplay between the evolving currents and the disordered thresholds. Actually, as can be

readily seen in Fig. 1, fluctuations are strongly asymmetric around the average, which immediately implies a non-Gaussian distribution of η , possibly including nontrivial correlations. Despite these difficulties one can perform the integral in certain limit, up to certain energy cutoff E_\times below which fluctuations of the energy are negligible. We have

$$\begin{aligned} \mathcal{P}_\tau(E, L) &= \tau^{-1} \int_0^\tau dt \delta[L^{-\sigma} t^\alpha + \eta(t) - E] \\ &= \tau^{-1} L^{\sigma/\alpha} E^{-1+1/\alpha} \int_0^{\tau(L^\sigma E)^{1/\alpha}} ds \\ &\quad \times \delta[s^\alpha + \eta(L^{\sigma/\alpha} E^{1/\alpha} s)/E - 1], \end{aligned} \quad (3)$$

and thus, keeping only the lowest-order term, we arrive at

$$\mathcal{P}_\tau(E, L) \sim \tau^{-1} L^{\sigma/\alpha} E^{-1+1/\alpha} \quad (4)$$

for $\tau/(L^\sigma E)^{1/\alpha} \gg 1$. This immediately leads to the existence of a characteristic energy scale $E_\times \sim L^{-\sigma} \tau^\alpha$ above which energy fluctuations dominate the statistics. It is clear that the details of the noise statistics (including the distribution and temporal correlations) would be required to obtain the specific mathematical form of the dissipated energy distribution above the characteristic energy E_\times . For the RFM we have an algebraic growth with exponent $\alpha \approx 2$ (see Fig. 1), so we expect to have an energy distribution decaying as $\sim E^{-1/2}$ for energies $E < E_\times$.

We are interested here in the distribution statistics after complete breakdown is attained. The characteristic time to total failure is expected to scale with system size as $T_{\text{break}} \sim L^z$, where z is the dynamic exponent. From Eq. (4) the energy statistics after failure, $\mathcal{P}(E, L) \equiv \mathcal{P}_{\tau=T_{\text{break}}}(E, L)$, reads

$$\mathcal{P}(E, L) \sim L^{-z+\sigma/\alpha} E^{-1+1/\alpha}, \quad (5)$$

for energies below a crossover energy $E_\times \sim L^{\alpha z - \sigma}$.

Figure 3 shows the probability distribution $\mathcal{P}(E, L)$ with statistics collected up to total failure for the global dissipated energy introduced above. Two regions can be readily distinguished. The low-energy statistics is in excellent agreement with a power-law decay $\sim E^{-1/2}$ over several decades in energy. Similar behavior is observed in Fig. 4 for the macroscopic energy measure defined in Eq. (1).

The dependence on system size of the numerical data observed in Figs. 3 and 4 can be better characterized by means of a finite-size scaling analysis. The behavior of the energy distribution suggests the scaling ansatz

$$\mathcal{P}(E, L) \sim E^{-\beta_b} L^{-\kappa} \mathcal{G}(E/E_\times), \quad (6)$$

where the scaling function $\mathcal{G}(u) \sim \text{const}$ for $u \ll 1$ and becomes $\mathcal{G}(u) \sim u^{\beta_b - \beta_a}$ for $u \gg 1$. β_a and β_b are the scaling exponents of the distribution above and below the crossover, respectively. The crossover energy scales with system size as $E_\times \sim L^D$ with some critical exponent D .

We can now make use of the theoretical relation we derived in Eq. (5) to prove that the two scaling exponents κ and D are not independent. Comparing Eqs. (6) and (5) one finds that the following scaling relations must be satisfied:

$$D = \alpha z - \sigma,$$

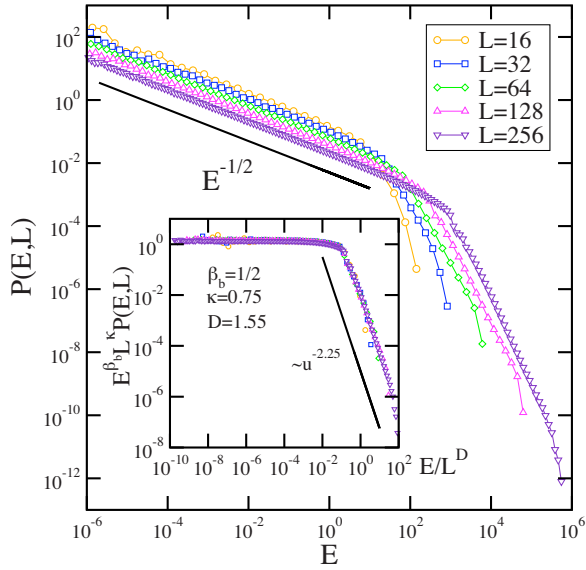


FIG. 3. (Color online) Probability distribution of the global dissipated energy for different system sizes. The low-energy region decays as a power law with exponent $\beta=1/2$ and shows a crossover at E_{\times} . The inset shows data collapse according to Eq. (6). The values of κ and D are in good agreement with the expected relation $D=\alpha\kappa$. Logarithmic binning has been employed.

$$\kappa = z - \sigma/\alpha,$$

$$\beta_b = 1 - 1/\alpha, \quad (7)$$

which immediately imply that $D=\alpha\kappa$. Also, according to our estimate $\alpha=2$ from Fig. 1 we should have $\beta_b=1/2$. This

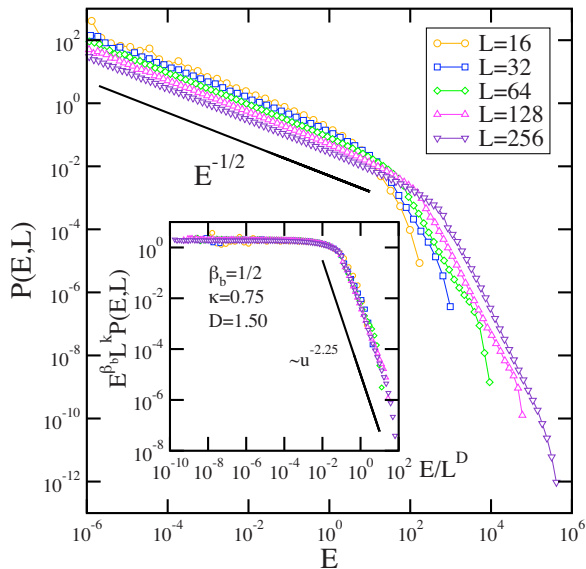


FIG. 4. (Color online) Probability distribution of macroscopic dissipated energy, Eq. (1), for different system sizes and the corresponding data collapse (inset). The same behavior and exponents as in the global definition are found

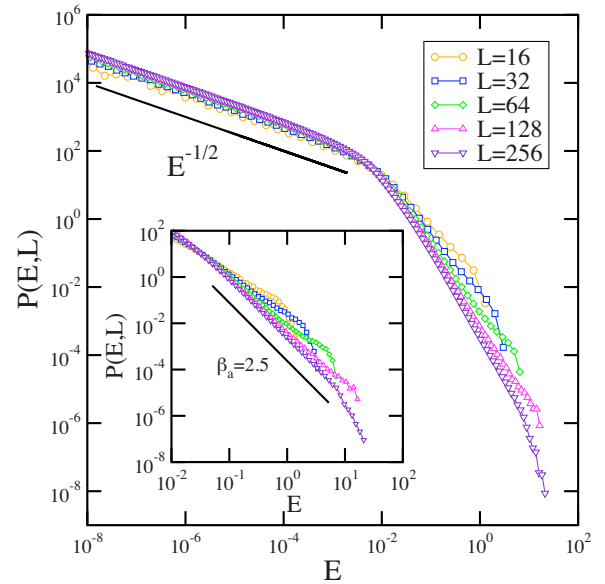


FIG. 5. (Color online) Probability distribution of microscopic dissipated energy, Eq. (2), for different system sizes. The inset shows a zoom of the high-energy region which decays with an exponent around $\beta=2.5$ over two decades for the largest system. Data show strong finite-size effects and do not obey good scaling behavior.

reduces the number of free exponents needed to achieve a good data collapse.¹

The insets of Figs. 3 and 4 show a data collapse according to Eq. (6) with exponents $\kappa=0.75(4)$, $D=1.55(5)$ and $\kappa=0.75(4)$, $D=1.50(5)$, respectively, and the energy exponent below the crossover $\beta_b=1/2$. The fit of the scaling function for $u \gg 1$ corresponds to the difference $\beta_b - \beta_a = -2.25(2)$, and implies that the scaling exponent of the energy distribution above the crossover is $\beta_a = 2.75(2)$, identical within error bars for both energy measures. This exponent is to be compared with the one calculated by Pradham *et al.* for the electric power dissipation in the high-energy region for the diamond lattice in Ref. [15], where they report $\beta=2.7$ over two decades of energy. The macroscopic energy defined in Eq. (1) exhibits not only the same behavior but the same exponents in the two regions, indicating that both definitions are completely equivalent. However, as we show below this is not the case for the microscopic energy statistics.

Figure 5 shows the behavior of the microscopic energy defined in Eq. (2). Recall that this measure is intended to collect only those contributions to the released energy coming from sites participating in the failure avalanche. We find that in the low-energy region the distribution also decays as $P(E,L) \sim E^{-1/2}$. However, in this case we observe that the probability does not seem to depend significantly on system size, $\kappa \approx 0$. Correspondingly, $D=\alpha\kappa \approx 0$ and the crossover energy E_{\times} does not vary with system size. The lack of sys-

¹We can also determine the dynamic exponent $z=1.75(3)$ by counting the average number of avalanches taking place before total failure in a system of lateral size L , which should scale as $T_{\text{break}} \sim L^z$. It is interesting to note that the specific value of z is not required to produce the data collapse in Eq. (6).

tem size dependence of the microscopic energy may be related to the fact that the macroscopic and global estimators are sensible to the whole volume of the system, while the microscopic energy is not. The inset of Fig. 5 shows a zoom of the high-energy region, where strong finite-size effects are demonstrated by the variation of the exponent β_a with system size. Data in Fig. 5 obviously fail to exhibit finite-size scaling.

It is worth stressing here that the PDF for all three energy definitions exhibits identical scaling behavior at low energies, $\sim E^{-1/2}$, and is robust to changes in system size and lattice type. This universality arises from the t^2 growth law of the dissipated energy, which is a feature shared by all three definitions for any system size and lattice geometry. However, the lack of scaling behavior with system size of the microscopic energy has a direct impact on the high-energy regime of its probability distribution.

B. Nonstationarity and signatures of imminent failure

The temporal series of the dissipated energy in the fuse model are highly nonstationary, as can be easily noticed in Fig. 1, and so the probability density $\mathcal{P}_\tau(E, L)$ depends explicitly on the observation time τ . This has been claimed to be useful to signal the onset of catastrophic failure [14,15], with evident practical applications for diagnosing damage in loaded materials.

In [15] the power dissipation avalanche distribution for the entire breakdown process was compared with that obtained only in a very narrow window around breakdown. In order to do this, those authors first computed the average over disorder samples of the number of fuses $\langle N_{\text{break}} \rangle$ blown before catastrophic failure and, for every realization, collected statistics from events after almost $\langle N_{\text{break}} \rangle$ fuses have blown. A possible drawback of that procedure is that, since the time required to reach total failure varies greatly among different disorder samples, one is mixing realizations that are very close to complete failure with others that are, say, half-way into it, which obey a different statistics.

Our procedure to obtain the statistics differs significantly from that used in Refs. [14,15] and has the advantage that it is not affected by this undesired effect. Moreover, in contrast to [14,15] we want to compare here the distribution of released energy until breakdown with that obtained when the system is at the very beginning of its evolution and how it changes as we approach failure. We proceed as follows. For each disorder realization we let the system evolve up to total breakdown, which gives the corresponding T_{break} for that particular disorder realization. We then compare the collected statistics with that observed for that particular disorder realization up to two intermediate times $\tau = T_{\text{break}}/8$ and $T_{\text{break}}/2$, that is, with the probability density when only the first one-eighth and one-half of the failure avalanches are counted, respectively, so that we collect statistics from realizations at the same evolution stage.

For each observation time, the probability density $\mathcal{P}_\tau(E, L)$ decays as $\sim E^{-1/2}$ until the crossover energy $E_\times(\tau, L)$. In Fig. 6 we plot the behavior of the distribution for the macroscopic energy, Eq. (1), for different system

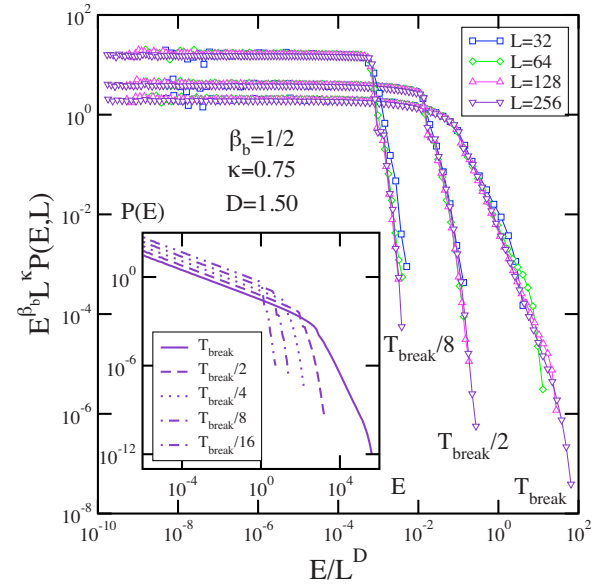


FIG. 6. (Color online) Macroscopic energy distribution for different final observation times. The same exponents collapse the distribution independently of the observation time but the slope of the high-energy tail is shifted to larger values when one measures further away from the breakdown instant. The inset shows the energy distribution for more intermediate observation times for $L=256$. It can be clearly observed the slope change at breakdown.

sizes and different observation times, rescaled according to Eq. (6). It can be observed that, while the crossover shifts to larger energy values as we approach complete breakdown, the scaling exponent in the second region is conserved as we increase the observation time. However, an abrupt change of exponent is observed only at the breakdown time T_{break} . This effect is perhaps better visualized in the inset of Fig. 6 where we plot the distribution data (unscaled) for the largest system $L=256$ and different observation times. Despite that we used a different measure of the dissipated energy and a different way to collect events these results are in agreement with the crossover picture between the two limiting behaviors reported in Refs. [14,15]. This indicates that nonstationary effects of the dissipated energy's temporal signal may actually be useful to characterize damage in stressed materials.

C. Finite driving rate

The lack of time scale separation in real experiments has been suggested [17] as a possible reason for the discrepancy with the typical exponents found in numerical simulations of quasistatic models. In order to investigate this point we have studied the RFM under finite driving rates, so that the model evolution is no longer quasistatic. We have analyzed both stress and strain loading conditions and our results were not affected by the loading mode we used. For the sake of brevity here we only report on our results for the latter.

Strain is applied on the system by imposing a small potential drop between the bus bars in such a way that all the fuses are initially below threshold. The voltage is then increased at a fixed rate dV/V letting all the fuses over threshold burn, instead of the slow driving setup studied above. As

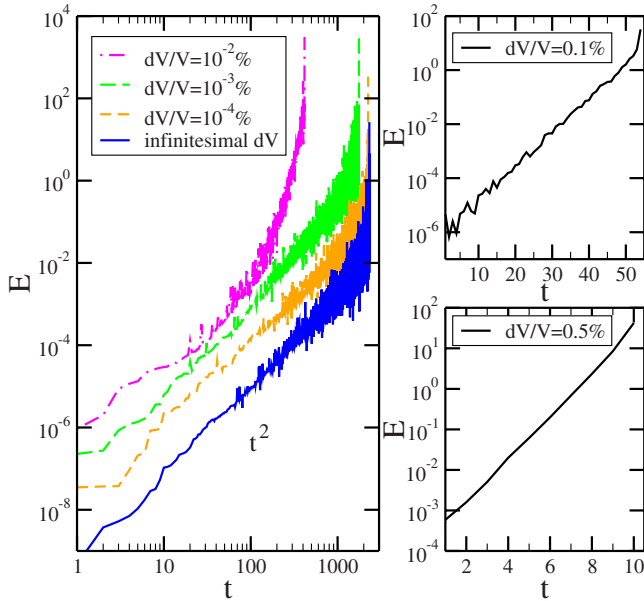


FIG. 7. (Color online) Temporal evolution of microscopic energy in an $L=128$ diamond lattice for several finite driving rates. On the left panel, it can be observed that, as the driving is increased, the energy starts to deviate from t^2 growth. On the right panels, one can see that, for large enough driving, the energy grows exponentially in time. Note the linear-log scale in the latter.

before, an avalanche is defined as all the fuses burnt between two consecutive voltage increments. In this setup, we can still observe an effective time scale separation at the early stages of the evolution, while potential increments are small.

Figure 7 summarizes our numerical results for the time evolution of the microscopic dissipated energy, Eq. (2), at different strain rates in diamond lattices of linear size $L=128$. We observe that a power-law trend $E \sim t^\alpha$ is satisfied with a larger exponent α as the strain rate increases. If the strain rate is large enough (about $dV/V=0.01\%$) the evolution is no longer described by a power law, but becomes exponential in time. The same behavior is observed if either the macroscopic or global energy is used.

According to our simple calculation in Eq. (4), we expect that, in the limit of exponential growth, $\alpha \gg 1$, the PDF of the dissipated energy becomes $\mathcal{P}_\tau(E) \sim E^{-1}$ for $E \ll E_\times$. We observe that the crossover energy E_\times diverges as the strain rate is increased. In Fig. 7 one can clearly see that when we increase the strain rate the energy fluctuations become much smaller. In fact, fluctuations are negligible for the whole temporal (energy) range for large enough driving rates, when the exponential growth sets in (see Fig. 7). This means that the falloff tail of the distribution corresponding to energies $E \gg E_\times$ is completely washed out in the case of large enough strain rates. Therefore we expect the dissipated energy probability to be

$$\mathcal{P}(E) \sim E^{-1} \quad (8)$$

if we let the system evolve up to complete breakdown, $\tau = T_{\text{break}}$, as well as for any other intermediate times.

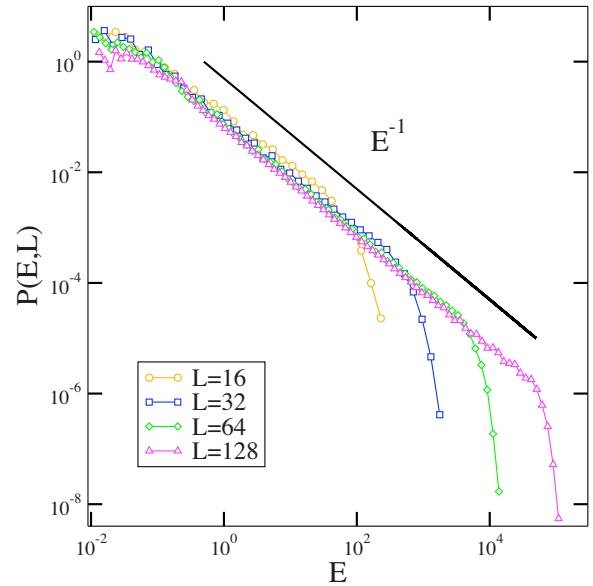


FIG. 8. (Color online) Macroscopic energy distribution for $L=16, 32, 64,$ and 128 diamond lattices under finite strain increments $dV/V=10^{-1}\%$. A single power-law regime with the predicted exponent $\beta=1$ is observed over the whole range of energies up to a finite-size cutoff.

In Fig. 8 we show the PDF of the macroscopic dissipated energy under a strain loading rate $dV/V=0.1\%$ measured for all events up to total failure in the diamond lattice for different system sizes. Identical results are obtained for the global energy estimator (not shown). Our numerical results are in excellent agreement with the prediction for finite loading rates in Eq. (8). The probability distribution for the microscopic energy also scales as E^{-1} for the whole range of energies in the case of finite driving (not shown), but the crossover energy shows no dependence with system size, in agreement with our above discussed results $D \approx 0$.

The conclusion is that the lack of time scale separation leads to a significant change in the distribution of the dissipated energy in the fuse model, as it should be expected. From a physical point of view there are strong differences in the system dynamics in the case of infinitesimal driving as compared with finite driving. If the system is driven at finite rates, relaxation to one of the infinitely many metastable configurations is not reached before a new perturbation acts on the system. This gives rise to a highly nonlinear superposition of cascades of released energy instead of individual well-defined avalanche events. A finite driving rate generically leads to a growth of the dissipated energy at a much faster rate than the usual quasistatic dynamics, possibly exponential for any finite driving rate in large enough systems. In turn, this fast growth takes the crossover energy E_\times to exponentially large values. The result is that the range of energies in which the PDF of the dissipated energy is described by Eq. (8) becomes very large, actually covering the whole range of energies.

IV. DISCUSSION

We have studied the RFM for fracture under strain loading conditions. We have focused on the dissipated energy in

order to test the validity of the model to account for the AE statistics observed in real experiments in loaded materials. Different ways to define the released energy have been discussed, including a microscopic quantity that takes into account just the energy losses at each broken bond during an avalanche.

Our results indicate that, for quasistatic dynamics, the dissipated energy statistics exhibits two very different regions depending on the energy scale one is looking at. These two scaling regions are separated by a typical energy $E_{\times} \sim L^{\alpha z - \sigma}$ and obey finite-size critical behavior. The low-energy region, for $E < E_{\times}$, is well described by a power-law decay $\mathcal{P}(E) \sim E^{-1/2}$, which is robust and independent of lattice geometry. We gave a simple scaling argument showing that this robustness is linked to the generic t^2 growth law of the dissipated energy; a feature shared by all the energy estimators we studied on any system size and lattice type, and that it is directly linked to the quasistatic nature of the model. The statistics above the typical energy $E > E_{\times}$ crosses over to $\mathcal{P}(E) \sim E^{-2.75}$ and ranges several decades in energy.

Apart from scaling factors, the three energy definitions used here were expected to show similar statistics. However, while the behavior of macroscopic and global energies can be captured by the same scaling exponents and the high-energy region exponent is well defined, this is not the case for the microscopic energy, which, although it obeys the same scaling form, shows no system size dependence and a different (size-dependent) exponent for the high-energy region is obtained. Regarding the microscopic energy we introduced here, one must admit that scaling in the high-energy region is not satisfying in general terms. Not only does the

numerical value of the exponent depend on the lattice size and fail to exhibit finite-size scaling, but also the scaling region covers a very narrow energy range. This should be particularly relevant when comparing with real fracture experiments, which have shown that dissipated energy participating in AE is not released all across the sample, but, quite the opposite, localized at microfractures [9,10].

Finally, we also studied the fuse model at finite driving rates. It is an often expressed belief that relaxing the quasistatic condition might lead to β exponents that compare better with experiments. We showed that under finite driving the cutoff energy diverges exponentially, so that the scaling $\mathcal{P}(E) \sim E^{-1}$ dominates the whole energy range at any given time for large enough driving rates (possibly for any finite driving rate in large enough systems). The conclusion is that relaxing the quasistatic condition cannot give account of experiments, where β typically ranges between 1.2 and 2.0, depending on the material.

The evidence we have up to now about the RFM indicates that it might well be the case that other aspects essential for a quantitative account of AE energy exponents in real materials, like plasticity, dislocations, friction, damping of acoustic waves, etc., are missing in the admittedly oversimplified fuse model.

ACKNOWLEDGMENTS

Financial support from the Ministerio de Educación y Ciencia (Spain) under Project No. FIS2006-12253-C06-04 is acknowledged. C.B.P. is funded by the FPU Program of the Ministerio de Educación y Ciencia (Spain).

-
- [1] J. P. Sethna and C. R. Dahmen, *Nature (London)* **410**, 242 (2001).
 - [2] P. Diodati, F. Marchesoni, and S. Piazza, *Phys. Rev. Lett.* **67**, 2239 (1991).
 - [3] P. A. Houle and J. P. Sethna, *Phys. Rev. E* **54**, 278 (1996).
 - [4] S. Field, J. Witt, F. Nori, and X. Ling, *Phys. Rev. Lett.* **74**, 1206 (1995).
 - [5] G. Durin and S. Zapperi, *Phys. Rev. Lett.* **84**, 4705 (2000).
 - [6] M. C. Miguel, A. Vespignani, and S. Zapperi, *Nature (London)* **410**, 667 (2001).
 - [7] A. Petri, G. Paparo, A. Vespignani, A. Alippi, and M. Costantini, *Phys. Rev. Lett.* **73**, 3423 (1994).
 - [8] L. I. Salminen, A. I. Tolvanen, and M. J. Alava, *Phys. Rev. Lett.* **89**, 185503 (2002).
 - [9] A. Garcimartín, A. Guarino, L. Bellon, and S. Ciliberto, *Phys. Rev. Lett.* **79**, 3202 (1997).
 - [10] A. Guarino, A. Garcimartín, and S. Ciliberto, *Eur. Phys. J. B* **6**, 13 (1998).
 - [11] A. Guarino *et al.*, *Eur. Phys. J. B* **26**, 141 (2002).
 - [12] C. Maes, A. Van Moffaert, H. Frederix, and H. Strauven, *Phys. Rev. B* **57**, 4987 (1998).
 - [13] L. I. Salminen *et al.*, *Europhys. Lett.* **73**, 55 (2006).
 - [14] S. Pradhan, A. Hansen, and P. C. Hemmer, *Phys. Rev. Lett.* **95**, 125501 (2005).
 - [15] S. Pradhan, A. Hansen, and P. C. Hemmer, *Phys. Rev. E* **74**, 016122 (2006).
 - [16] V. Kuksenko, N. Tomilin, and A. Chmel, *J. Stat. Mech.: Theory Exp.* (2005) P06012.
 - [17] M. J. Alava, P. K. V. V. Nukala, and S. Zapperi, *Adv. Phys.* **55**, 349 (2006).
 - [18] K. J. Måløy, S. Santucci, J. Schmittbuhl, and R. Toussaint, *Phys. Rev. Lett.* **96**, 045501 (2006).
 - [19] J. Davidsen, S. Stanchits, and G. Dresen, *Phys. Rev. Lett.* **98**, 125502 (2007).
 - [20] E. Bouchaud, *J. Phys.: Condens. Matter* **9**, 4319 (1997).
 - [21] S. Ramanathan and D. S. Fisher, *Phys. Rev. B* **58**, 6026 (1998).
 - [22] E. Katzav and M. Adda-Bedia, *Europhys. Lett.* **76**, 450 (2006).
 - [23] D. Bonamy, L. Ponson, S. Prades, E. Bouchaud, and C. Guillot, *Phys. Rev. Lett.* **97**, 135504 (2006).
 - [24] E. Katzav, M. Adda-Bedia, and B. Derrida, *Europhys. Lett.* **78**, 46006 (2007).
 - [25] L. de Arcangelis, S. Redner, and H. J. Herrmann, *J. Phys. (Paris), Lett.* **46**, 585 (1985).
 - [26] A. Hansen, E. L. Hinrichsen, and S. Roux, *Phys. Rev. Lett.* **66**, 2476 (1991).
 - [27] A. Hansen, E. L. Hinrichsen, and S. Roux, *Phys. Rev. B* **43**, 665 (1991).

- [28] L. de Arcangelis and H. J. Herrmann, *Phys. Rev. B* **39**, 2678 (1989).
- [29] E. T. Seppälä, V. I. Räsänen, and M. J. Alava, *Phys. Rev. E* **61**, 6312 (2000).
- [30] S. Zapperi, P. K. V. V. Nukala, and S. Šimunović, *Phys. Rev. E* **71**, 026106 (2005).
- [31] M. J. Alava, P. K. V. V. Nukala, and S. Zapperi, *J. Stat. Mech.: Theory Exp.* (2006) L10002.
- [32] Phani Kumar V. V. Nukala, S. Zapperi, and S. Šimunović, *Phys. Rev. E* **74**, 026105 (2006).
- [33] P. K. V. V. Nukala, S. Šimunović, and S. Zapperi, *J. Stat. Mech.: Theory Exp.* (2004) P08001.
- [34] A. Hansen and P. C. Hemmer, *Phys. Lett. A* **184**, 394 (1994).
- [35] S. Zapperi, P. Ray, H. E. Stanley, and A. Vespignani, *Phys. Rev. Lett.* **78**, 1408 (1997).
- [36] S. Zapperi, P. Ray, H. E. Stanley, and A. Vespignani, *Phys. Rev. E* **59**, 5049 (1999).
- [37] S. Zapperi, P. K. V. V. Nukala, and S. Šimunović, *Physica A* **357**, 129 (2005).
- [38] S. Zapperi and P. K. V. V. Nukala, *Int. J. Fract.* **140**, 99 (2006).
- [39] D. R. Otomar, I. L. Menezes-Sobrinho, and M. S. Couto, *Phys. Rev. Lett.* **96**, 095501 (2006).
- [40] G. G. Batrouni and A. Hansen, *J. Stat. Phys.* **52**, 747 (1988).
- [41] P. K. V. V. Nukala and S. Šimunović, *J. Phys. A* **36**, 11403 (2003).
- [42] P. K. V. V. Nukala, S. Šimunović, and M. N. Gudatti, *Int. J. Numer. Methods Eng.* **62**, 1982 (2005).
- [43] M. Minozzi, G. Caldarelli, L. Pietronero, and S. Zapperi, *Eur. Phys. J. B* **36**, 203 (2003).